Elaboration of Ce:(Lu,Gd) 3 Al 5 O 12 -Al 2 O 3 transparent nanoceramics through full glass crystallization for high-power warm white LED/LD lighting

Jie Fu, Ying Zhang, Shaowei Feng, Yongchang Guo, Yafeng Yang, Cécile Genevois, Emmanuel Véron, Hui Wang, Mathieu Allix, Jianqiang Li

Elaboration of Ce:$(Lu,Gd)_3Al_5O_{12}$-Al_2O_3 transparent nanoceramics through full glass crystallization for high-power warm white LED/LD lighting

Jie Fu[a,b,d], Ying Zhang[a,d], Shaowei Feng[a,d], Yongchang Guo[a,d], Yafeng Yang[a,d], Cécile Genevois[c], Emmanuel Veron[c], Hui Wang[a,d], Mathieu Allix[c,*], and Jianqiang Li[a,b,d,*]

[a]*State Key Laboratory of Multiphase Complex Systems, Institute of Process Engineering, Chinese Academy of Sciences, Beijing 100190, China*

[b]*School of Materials Science and Engineering, University of Science and Technology Beijing, Beijing 100083, PR China*

[c]*CNRS, CEMHTI UPR 3079, Univ. Orléans, 45071 Orléans, France*

[d]*University of Chinese Academy of Sciences, Beijing 100049, China*

ABSTRACT

Transparent Ce:$Lu_3Al_5O_{12}$ (Ce:LuAG) phosphor ceramics have emerged as promising color conversion materials in high-power white lighting due to their relatively high quantum efficiency, high thermal stability and low thermal quenching. However, the shortage of red spectral composition and expensive price are preventing the application of Ce:LuAG phosphor ceramics in high-quality white lighting. In this work, $(Lu,Gd)_3Al_5O_{12}$-Al_2O_3 (LuGAG-Al_2O_3) nanoceramics in which Gd^{3+} is selected to partially replace Lu^{3+}, were prepared through the full glass crystallization from a 72 mol.% Al_2O_3-28 mol.% (0.8 Lu_2O_3-0.2 Gd_2O_3) bulk glass. These ceramics are composed of nanoscale grains (less than 50 nm) with a fully dense biphasic three-dimensional network nanostructure, that allows outstanding transparency (82.3%@780 nm) and excellent mechanical properties (hardness is 23.4 GPa). Compared with Ce:LuAG-Al_2O_3 transparent nanoceramics, the emission spectrum of transparent Ce:LuGAG-Al_2O_3 nanoceramics shows a substantial red shift (505 nm→570 nm), which effectively supplement the red light lacking in Ce:LuAG ceramics. And the transparent Ce:LuGAG-Al_2O_3 nanoceramics exhibit a maximum quantum efficiency of 81.4% and excellent thermal stability (87.6%@423 K), indicating potential for high-power white lighting. When used in high-power LED and

LD lighting, Ce:LuGAG-Al_2O_3 transparent nanoceramics achieve continuous adjustable changes from green light to orange-yellow light, and furthermore provide high quality warm white lighting with low color temperature, high color rendering index, and excellent luminous efficiency. Especially, integrated to blue-emitting InGaN chips (10 W), 0.8%Ce:LuGAG-Al_2O_3 transparent nanoceramics generate state of the art performance regarding warm white lighting (4526 K, 73.5, 143.98 $lm \cdot W^{-1}$). Under blue laser-diode excitation (5 $W \cdot mm^{-2}$), transparent 0.8%Ce:LuGAG-Al_2O_3 nanoceramics also demonstrate optimum performance for warm white lighting (4611 K, 65.4, 161.29 $lm \cdot W^{-1}$). Combining the facile and moderate elaboration process through full glass crystallization, the transparent Ce:LuGAG-Al_2O_3 nanoceramics reported in this paper are therefore regarded as promising color converters candidates for high-power warm white LED/LD lighting.

Keywords: glass crystallization; LuGAG-Al_2O_3 transparent nanoceramics; red shift; high-power WLEDs/LDs

1. Introduction

Solid-state lighting (SSL) technology is rapidly developing in modern industrial world due to its long service life, high efficiency and environmental protection advantages.[1-2] It is widely used in various scenes such as projection displays, automobile headlights, industrial production, and long-distance lighting.[3] High-power, high-brightness white light-emitting diodes (WLED) and laser lighting technology put forward new requirements for the service stability of color conversion materials.[4-5] Phosphor ceramics rise rapidly because of their unique advantage of withstanding high power excitation density.[6-7] Ce:YAG phosphor ceramics have been widely studied as color converters for WLED and LD-driven white lighting.[8-12] However, single phase Ce:YAG phosphor ceramics are limited by the limited thermal stability and narrow spectrum, that leads to serious thermal quenching, dificient color rendering index (CRI) and high correlation color temperature (CCT).[13] In comparison, Ce:LuAG phosphor ceramics are regarded as suitable candidates for high power density pump illumination and display, due to their low thermal quenching

property, high thermal conductivity and high quantum efficiency (>90%).[14-15] Ma et al.[16] successfully prepared LuAG transparent ceramics with different Ce^{3+} doping concentrations by vacuum sintering. Ce:LuAG transparent ceramics emit yellow-green light when combined with LED chip, and exhibit luminous efficiency up to 223.4 $lm \cdot W^{-1}$, and maximum color rendering index of 55.8. Xu et al.[17] synthesized Ce:LuAG translucent phosphor ceramics by spark plasma sintering (SPS) technology. The obtained phosphor ceramics show external quantum efficiency up to 77%, good thermal conductivity (6.3 $W \cdot m^{-1} \cdot K^{-1}$) and high reliability (98.1% after 1000 h). Zhang et al.[18] prepared Ce:LuAG phosphor ceramics at high temperature. The resulting phosphor ceramics show good thermal stability (90%@450 K) and high luminous efficiency (~200 $lm \cdot W^{-1}$). The above results show that Ce:LuAG phosphor ceramics have great application potential in high power white lighting.

However, the emission spectrum of Ce:LuAG phosphor ceramics is mainly located in the green light region (<520 nm), which prevent high-quality white light illumination under the excitation of blue LED/LD. Moreover, high-purity Lu_2O_3 powder, one of the starting materials of Ce:LuAG, is very expensive. As the luminescence characteristics of Ce:LuAG phosphor ceramics are related to the crystal environment around Ce^{3+}, the emission light can be tuned by adjusting the material composition and energy band structure. One method is to distort the cubic symmetry around the rare earth element (RE) by increasing or decreasing the ion radius or introducing impurity atoms into the crystal structure.[13] Gd^{3+} has been reported to have an important influence on the crystal band structure and energy state of Ce^{3+} in garnet ceramics. Qian et al.[19] showed that as the Gd^{3+} concentration was increased from 0 to 0.5 in $(Y_{1-x}Gd_x)_3Al_5O_{12}$, the PL emission spectra of Ce:GdYAG phosphors shifted from 542 nm to 575 nm under a 460 nm excitation. Shi et al.[20] also inserted Gd^{3+} in the YAG lattice which provided excellent color coordinates and CRI for warm white light illumination. Tanabe et al.[21] studied the optical properties of Ce:YAG glass ceramic phosphor for WLED, and found that the substitution of Y^{3+} by Gd^{3+} shifted the color of the emitted light closer to warm white. And, the price of pure

Gd_2O_3 powder is only 1/250 of the price of Lu_2O_3, facilitating Gd as an cost effective candidate for possible substitution in Ce:LuAG phosphor ceramics.[22]

The traditional powder sintering method for preparing phosphor ceramics require long and complex high temperature and high pressure treatments, and the harsh requirements for raw materials (particle size and distribution).[23] A simple, rapid and low-cost preparation method would be an interesting alternative. In recent years, the research on the preparation of transparent ceramics by the full crystallization of bulk glass has attracted great attention.[24] A variety of nanocrystalline transparent ceramic materials have been successfully prepared by low-temperature crystallization, such as Al_2O_3-ZrO_2-Re_2O_3 (Re=La, Gd, Y) system elaborated by Rosenflanz,[25] and Allix et al.[26-28] also prepared highly transparent $BaAl_4O_7$ and $Sr_3Al_2O_6$ ceramics with high density, thin grain boundaries, and excellent hardness and modulus properties. These materials also showed excellent phosphor properties via rare earth doping. In recent works, we synthesized Al_2O_3-Y_2O_3 and Al_2O_3-Lu_2O_3 glasses by containerless solidification process and successfully crystallized them into fully dense biphasic YAG-Al_2O_3 and LuAG-Al_2O_3 nanocrystalline ceramics with high transmittance.[29-30] Up to now, LuGAG transparent ceramics with nano sized grains has not been reported. The full glass crystallization method therefore appears as a promising route to elaborate Ce:LuGAG-based transparent phosphor ceramics.

In this paper, LuGAG-Al_2O_3 transparent biphasic nanoceramics were prepared by full glass crystallization method from a 72 mol.% Al_2O_3-28 mol.% (0.8 Lu_2O_3-0.2 Gd_2O_3) bulk glass synthesized by containerless solidification process. The microstructure, transmittance and mechanical properties of LuGAG-Al_2O_3 transparent nanoceramics were studied in details and the luminescent properties of the LuGAG-based nanoceramics with different Ce^{3+} concentrations were investigated. The influence of Gd^{3+} doping on the emission spectrum was especially examined and discussed. Last, the application of transparent Ce:LuGAG-Al_2O_3 nanoceramics in LED/LD lighting has been studied and analyzed. The results show that the substitution of Gd^{3+} for Lu^{3+}, leading to Ce^{3+}:LuGAG-Al_2O_3 materials, can reduce costs, effectively compensate for the lack of red light emission observed in

Ce^{3+}:LuAG and enlarge the color rendering index of ceramics, thereby improving the performance of Ce:LuAG phosphor ceramics for use in high-power warm white LED/LD lighting.

2. Experimental procedure

2.1. Sample preparation

High-purity commercial oxide powders Al_2O_3, CeO_2 and Gd_2O_3 (99.99%, Sinopharm chemical reagent co. ltd) and Lu_2O_3 (99.99%, Qiandong Rare Earth Group Co. Ltd) were used as starting materials. Our previous work reveals that an excessive Gd^{3+} substitution content (>20%) in LuAG ceramics will led to a rapid deterioration in the thermal stability of luminescence. Therefore, this paper adopted a 20% Gd^{3+} substitution concentration. And according to the works on $Lu_3Al_5O_{12}$-Al_2O_3 transparent nanoceramics, the ceramic sample has the highest transmittance when the Al_2O_3 content is 72%. The raw material powders were weighed according to the 72 mol.% Al_2O_3-28 mol.% ((1-x)(0.8 Lu_2O_3-0.2 Gd_2O_3), 2xCeO_2 with x=0, 0.001, 0.003, 0.005, 0.008, 0.01), then mixed in an agate mortar using ethanol as a dispersant, and dried in an air oven (50 °C, 2 h). An alloy mould was used to press the mixed raw material powders into pellets, which were then broken into 50-200 mg pieces. These were then placed in the nozzle of an aerodynamic levitation system and melted by CO_2 lasers at ~2600 °C. The CO_2 lasers were shut off to quench the samples to room temperature (~300 $℃·s^{-1}$). Glass beads with a diameter of ~2-5 mm were thus prepared and the glass beads were polished into disks (~1 mm thickness). After a single crystallization heat treatment in a muffle furnace using a temperature between 950 and 1300 °C, the glass disks were fully crystallized into transparent ceramics.

2.2. Microstructural and optical characterizations

The phase structure and crystallinity of samples were identified by X-ray powder diffraction (XRPD, Smartlab 9, Rigaku Corporation, Japan) with Cu Ka radiation, and data were collected from 5 to 90° (2θ). High resolution synchrotron XRPD was conducted at ambient temperature on the 11BM beamline (Argonne National Laboratory, USA). The sample was contained in a 0.8 mm Kapton capillary and spun during the measurement at incident wavelengths of 0.412791 Å. The thermal analysis

of the as-prepared glass samples was determined by differential scanning calorimeter (DSC, MULTI HTC 1600, Setaram, France) from room temperature up to 1200 °C, using argon as a purging gas and a heating rate of 10 °C·min^{-1}. The density of samples was measured with a gas pycnometer (PENTAPYC 5200e, Quanta, America). The grain size of the sample was obtained from the XRPD results using the Rietveld method through full spectrum fitting (the least squares method was used for fitting), and a strain correction factor was added to correct the obtained crystal size. The inline transmittance and absorption spectrum of the ceramic materials (1.0 mm thickness) was recorded using a UV-VIS-NIR spectrophotometer (Cary 5000, Agilent Inc., USA) in the 190-2500 nm wavelength range, and a Fourier-transform infrared spectrometer (Excalibur 3100, Varian Inc., USA) in the 2500~7000 nm wavelength range. The hardness and Young's modulus of ceramic materials were measured through a nanoindenter (G200, Keysight Technology) with a force of 350 mN and a displacement of 1000 nm. The Backscattered SEM images of ceramic samples were observed through scanning electron microscopy (SEM, JSM-7001F, JEOL, Japan). The nanostructures of the ceramic samples were characterized by transmission electron microscopy (TEM) using HRTEM and STEM-HAADF imaging modes and EDX elemental analyzes (line-scan and mapping). These experiments were performed on a ARM200 Cold FEG microscope (JEOL Ltd) operating at 200kV, equipped with a JEOL SDD CENTURIO EDS system and fitted with a double spherical aberration corrector. The samples were first prepared by mechanical polishing with a tripod and inlaid diamond discs to reach a thickness of 40μm. Thin foils were then obtained by argon ion milling (Gatan PIPS). The photoluminescence excitation (PLE) spectra, emission (PL) spectra and fluorescent decay curves of as-prepared ceramics were measured with a multifunctional fluorescence spectrometer (FluoroMax Plus, HORIBA, America). The quantum efficiency was tested by the integrating sphere fluorescence spectrometer (QE-2100, Otsuka Photo Electronics, Japan). The photoluminescence spectrum of LED/LD devices was measured by the OHSP-350M spectrum luminous flux analyzer (used with an integrating sphere with a diameter of

50 cm) produced by Hangzhou Rainbow Spectrum Optoelectronics Co., Ltd., and the measuring wavelength range was 380-780 nm.

3. Results and discussion

3.1. Preparation of transparent LuGAG-Al_2O_3 nanoceramics

Using the 72 mol.% Al_2O_3-28 mol.% (0.8 Lu_2O_3-0.2 Gd_2O_3) nominal composition, a transparent bulk material with a diameter of 3.0 mm (**Figure S1**) was prepared by melt-quenching using an aerodynamic levitation system as detailed in the experimental part. The corresponding XRPD pattern and SEM show that this transparent bulk material is mainly amorphous with a small amount of hexagonal (Gd,Lu)AlO_3 crystalline phase, we therefore consider this material as glass and denote it A(Lu,Gd)28 glass thereafter. The thermal behavior of A(Lu,Gd)28 glass was tested by DSC, as shown in **Figure S2**. The glass transition temperature (T_g) is 894±2 ℃ and the peak crystallization temperature (T_p) is 948±2 ℃. Therefore, the 950-1300 ℃ temperature range was selected to crystallize A(Lu,Gd)28 glass-based precursors and obtain the transparent ceramic materials.

The heat treated samples remain good transparency at the crystallization temperature of 1200 °C or below. At higher crystallization temperature, the samples began to lose their transparency. The XRPD patterns presented in **Figure 1(a)** show that all the transparent samples are completely crystalline and no glassy residue can be detected. The main diffraction peaks of transparent samples are highly consistent with the pattern of $(Lu,Gd)_3Al_5O_{12}$. Except for the $(Lu,Gd)_3Al_5O_{12}$ main crystal phase, the presence of Al_2O_3 is not obvious on laboratory XRPD measurements, but synchrotron powder diffraction data clearly demonstrate the presence of δ-Al_2O_3 (see **Figure 3(b)** and details later). When the crystallization temperature rised to 1100 °C or above, no more hexagonal (Lu,Gd)AlO_3 phase can be observed, probably due to the decomposition of this phase from glass matrix at higher temperatures. Therefore, the obtained transparent samples were ceramic materials[31] **Figure 1(b)** shows the density of A(Lu,Gd)28 glass-based precursors crystallized at different temperatures. Compared to the density of A(Lu,Gd)28 glasses 5.60±0.05 $g.cm^{-3}$, the density of the transparent ceramic materials increases significantly after crystallization. The density

of the obtained ceramic materials is 6.14±0.05 $g \cdot cm^{-3}$ when the crystallization temperature reaches 1100 °C, indicating that about a 10% volume shrinkage occurred during the crystallization process. With the further increase of crystallization temperature, the density of the transparent ceramic materials remain constant, indicating that completed crystallization has been reached and no further volume shrinkage occurred. Combining the XRPD results with strain effect correction, the fitted grain size of transparent ceramic materials is shown in **Figure 1(c)**. With the increase of crystallization temperature, grain sizes of transparent ceramics increase continuously (41±4 nm@1100 °C). The backscattered SEM images of transparent ceramic materials in **Figure S3** also confirm this evolution. **Figure 1(d)** shows the in-line transmission spectra of transparent ceramic materials obtained by crystallization of A(Lu,Gd)28 glasses at different temperatures. The results show that all the ceramics present outstanding transparency in the VIS-NIR and MIR regions. Especially, the transmittance of the ceramics crystallized at 1000 °C reaches the summit of 82.3%@780 nm. As the crystallization temperature further increases, the transmittance of ceramics in VIS region begins to gradually decreases, and become completely opaque at the temperature of 1300 °C. The grain size of ceramics continuely increases with temperature, enhancing the scattering between grains of LuGAG and Al_2O_3. In the mid infrared region, all the ceramics have almost the same transmittance since the light scattering effect is reduced at larger wavelengths. Compared to the maximum transmittance of transparent LuAG-Al_2O_3 nanoceramics (82.0%@780 nm) and LuAG single crystals (about 80%@780 nm) reported in literature,[30] the transmittance of the transparent ceramics obtained by replacing 20 mol% Lu_2O_3 with Gd_2O_3 is slightly improved. Therefore, transparent LuGAG-Al_2O_3 nanoceramics were successfully prepared by crystallization of A(Lu,Gd)28 glasses at different temperatures.

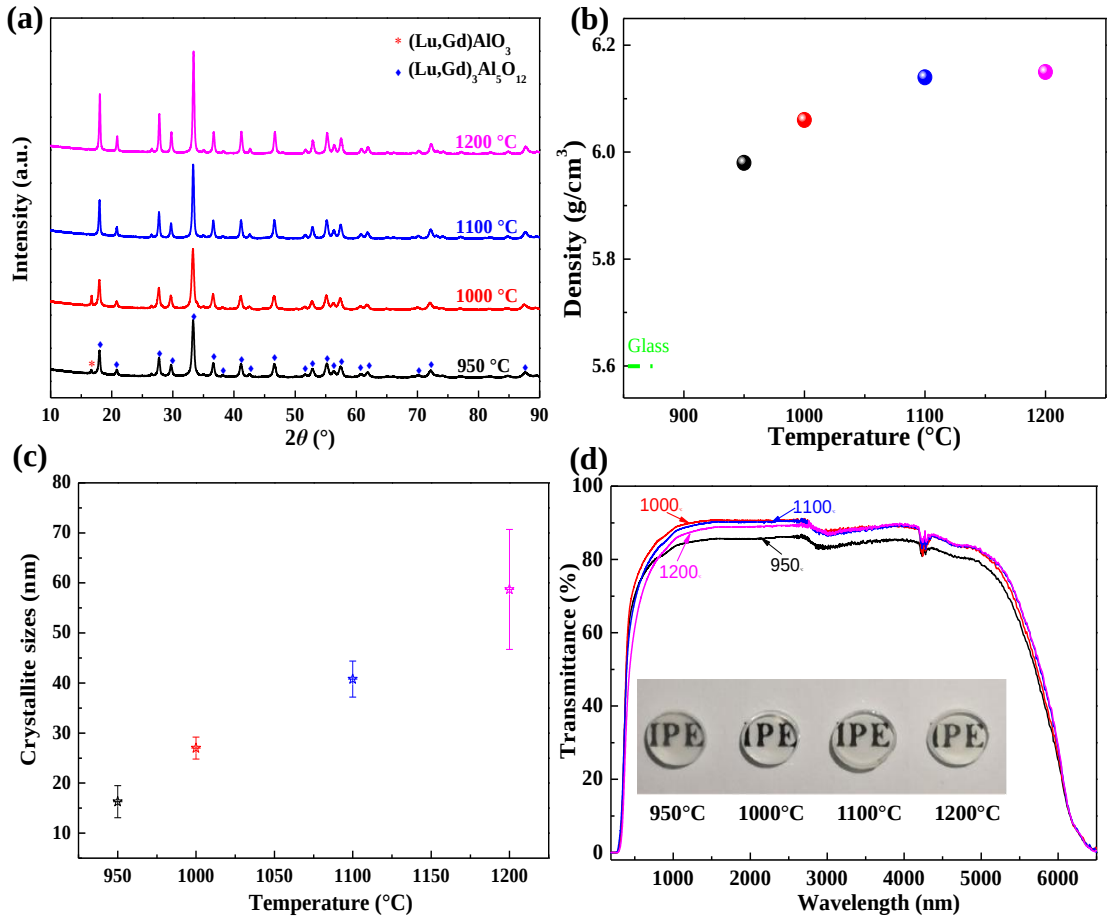

Figure 1. (a) XRPD patterns, (b) densities, (c) grain sizes and (d) in-line transmittance spectrum of transparent ceramics crystalized from A(Lu,Gd)28 glasses at 950 °C, 1000 °C, 1100 °C, and 1200 °C respectively for 2 h.

The mechanical properties of LuGAG-Al_2O_3 transparent ceramics were investigated and the results were given in **Figure 2**. **Figure 2(a)** shows the typical load-displacement curves of LuGAG-Al_2O_3 nanoceramics obtained at different crystallization temperatures. According to the load-displacement curves, the hardness and modulus of the sample can be calculated as shown in **Figure 2(b-c).** The hardness and Young's modulus of A(Lu,Gd)28 glasses are 15.7±1.9 GPa and 205.7±18.3 GPa, respectively. In comparison, the hardness and Young's modulus of the LuGAG-Al_2O_3 nanoceramics have significantly improved. When the crystallization temperature is 1100 °C, the hardness and Young's modulus of the transparent LuGAG-Al_2O_3 nanoceramics reach the maximum, which are 23.4±0.5 GPa and 320.2±1.5 GPa respectively. **Figure 2(d)** compares the hardness and Young's modulus of LuGAG-Al_2O_3 and LuAG-Al_2O_3 transparent nanoceramics, and LuAG transparent

microcrystalline ceramics. The results show that the Young's modulus of the three transparent ceramic materials is almost the same. However, LuGAG-Al_2O_3 and LuAG-Al_2O_3 transparent nanoceramics exhibit a hardness about 10% higher than that of the LuAG transparent microcrystalline ceramics. It can also be seen that the replacement of 20 mol% Lu_2O_3 with Gd_2O_3 does not generate a negative impact on the hardness and Young's modulus of nanoceramics. These good mechanical properties can benifit the service life of LuGAG-Al_2O_3 transparent nanoceramics.

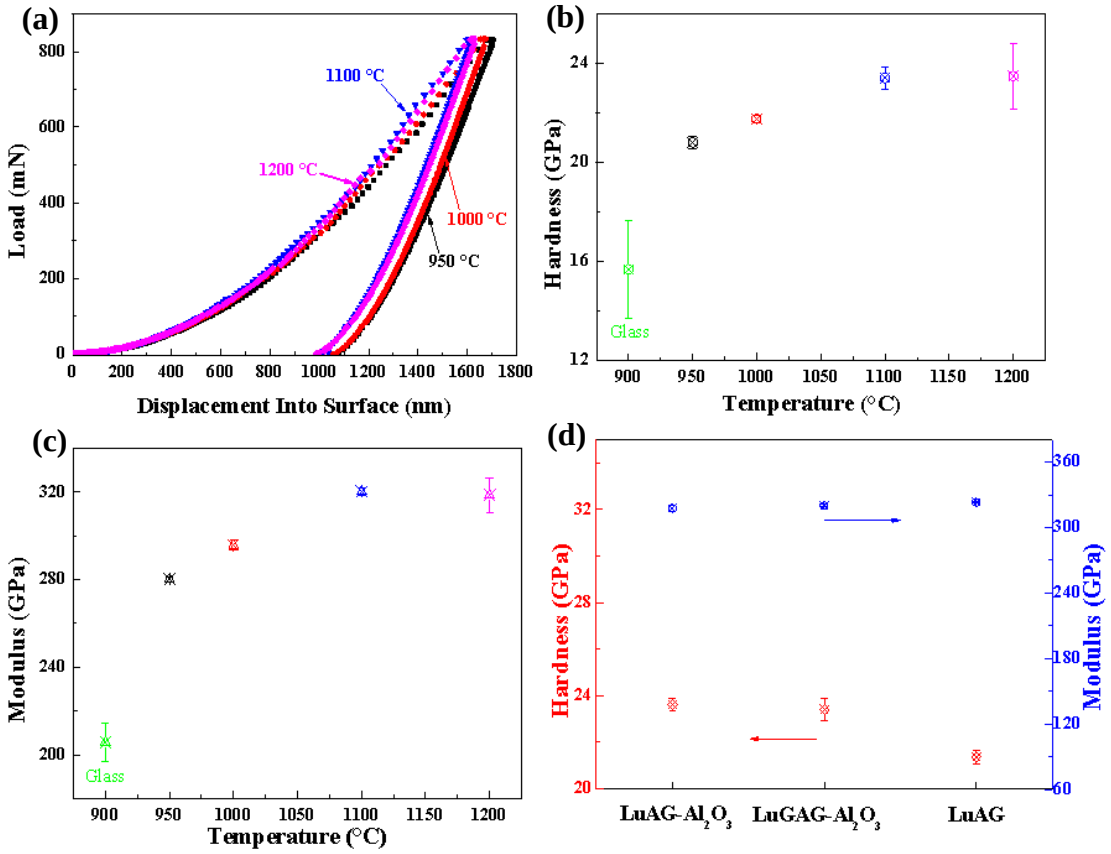

Figure 2. (a) Typical load-displacement curves and (b-c) the hardness and Young's modulus of transparent LuGAG-Al_2O_3 nanoceramics crystallized from A(Lu,Gd)28 bulk glasses at different temperatures, (d) comparison of hardness and Young's modulus of LuGAG-Al_2O_3 (1100 °C, 2 h), LuAG-Al_2O_3 (1100 °C, 2 h) and LuAG transparent ceramics (vacuum sintering).

Based on the above results, the crystallization of A(Lu,Gd)28 glasses is basically completed when the crystallization temperature reaches 1100 ℃. Therefore, the following part will mainly focus on transparent nanoceramic materials crystallized at 1100 ℃.

Figure 3(a) shows the in-line transmittance spectrum of transparent ceramic

materials crystallized from A(Lu,Gd)28 glasses at 1100 °C for 2 h. The photograph of this transparent ceramic sample is also embedded. It can be seen that this ceramic sample has excellent transmittance in VIS-NIR and MIR regions, and the transmittance is higher than 90% in the NIR region (1500-2700 nm). The absorption band near the wavelength of 3000 nm corresponds to the absorption of free hydroxyl (OH) group. **Figure 3(b)** shows the Rietveld refinement from synchrotron X-ray powder diffraction (SXPD) data acquired on the transparent ceramic material powder crystallized from A(Lu,Gd)28 glasses at 1100 °C for 2 h. In addition to the $(Lu,Gd)_3Al_5O_{12}$ garnet phase, there is clearly some δ-Al_2O_3 phase which was refined to 8.2(5) wt%. This phase composition is similar with our previous works on $Lu_3Al_5O_{12}$-Al_2O_3 and $Y_3Al_5O_{12}$-Al_2O_3 transparent nanoceramics.[29-30] The refined garnet crystallite size, using a fundamental approach, is 41.7(3) nm. Unfortunately, due to the close scattering factors of Lu and Gd, no composition refinement could be performed. However, the refined cell parameter, 11.97470(5) Å, corresponds well to a the value expected for $(Lu_{0.8}Gd_{0.2})_3Al_5O_{12}$ from Vegard's law when compared to $Lu_3Al_5O_{12}$ and $Gd_3Al_5O_{12}$. Combined with the STEM-HAADF image and EDS elemental maps in **Figure 4**, it can be seen that the transparent ceramics obtained after crystallisation at 1100 °C for 2 h are $(Lu,Gd)_3Al_5O_{12}$-Al_2O_3 (LuGAG-Al_2O_3) composite nanoceramics. **Figure 3(c,d)** show TEM micrographs of these LuGAG-Al_2O_3 composite nanoceramics. **Figure 3(c)** shows that the transparent ceramic is composed of dark and bright phases, and the grain size is at the nanoscale. No pores or microcracks can be seen. **Figure 3(d)** gives more details on the two phases configuration in the LuGAG-Al_2O_3 ceramic. **Figure 3(e)** shows that the grain size is slightly below 50 nm, in good agreement with the value obtained by Rietveld refinement from SXPD data, and the distribution is uniform. The FFT patterns in **Figure 3(f,g)** also indicate that the main crystal phase (dark phase) is $(Lu,Gd)_3Al_5O_{12}$ with garnet structure, and the second phase (bright phase) is Al_2O_3, which is distributed around the $(Lu,Gd)_3Al_5O_{12}$ crystals and can be indexed with δ-Al_2O_3 as proposed from SXPD observations. The existence of Al_2O_3 as a secondary phase effectively enables to release the shrinkage stress generated during the crystallization

process, which avoids the generation of microcracks, and thus enable to obtain a completely dense microstructure. On the other hand, it is reasonable to deduce that Al_2O_3 phase plays a role in limiting the growth of LuGAG crystals below 50 nm, resulting in the fully nano-grained ceramics.[32]

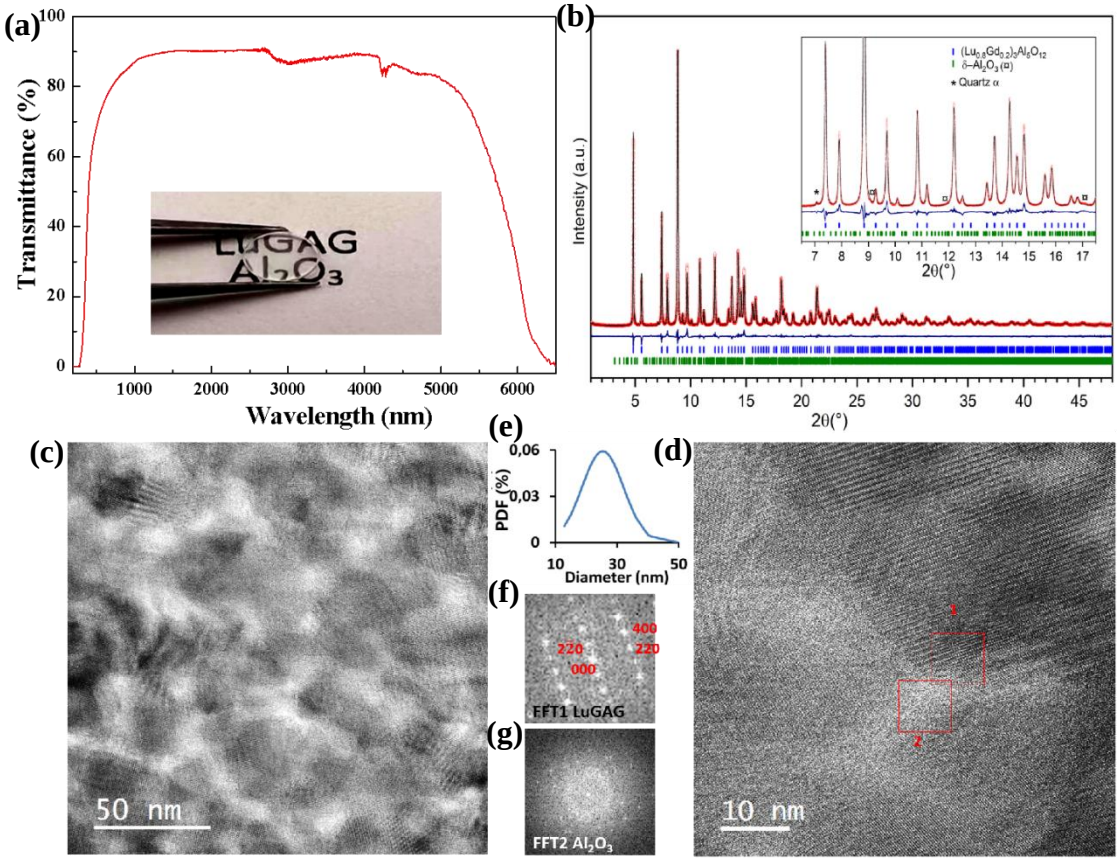

Figure 3. (a) In-line transmittance spectrum (the photograph of ceramic sample is embedded), (b) SXPD Rietveld refinement, (c,d) HRTEM micrographs, (e) grain size distribution curve (PDF is Probability Density Function), (f,g) FFT patterns (FFT1 LuGAG corresponds to Zone 1 in **Figure 3(d)**, FFT2 Al_2O_3 corresponds to Zone 2 in **Figure 3(d)**) of transparent ceramics crystallized from A(Lu,Gd)28 glasses at 1100 °C for 2 h.

3.2. Microstructure and luminescence properties of transparent Ce:LuGAG-Al_2O_3 nanoceramics

Figure 4 presents a STEM-HAADF micrograph along with EDS elemental mapping images of transparent 0.3%Ce:LuGAG-Al_2O_3 nanoceramics obtained by crystallization of A(Lu,Gd)28 bulk glasses with 0.3% Ce^{3+} at 1100 °C for 2 h. The STEM-HAADF image presented **Figure 4(a)** shows that the composition of the dark phase is Al_2O_3, while the atomic percentage of the elements in the bright phase is

consistent with that in the LuGAG garnet phase, where the proportion of Gd element is about 20 mol% of the overall Lu+Gd content, which is consistent with the proportion of raw materials. **Figure 4(b-g)** show that Lu, Gd and Ce three elements are distributed in the bright phase, while Al is distributed in the whole sample. However, the concentration of Al is higher in the dark phase area, which further indicates that the dark phase area corresponds to Al_2O_3 and the bright phase is assigned to the LuGAG garnet phase. These observations also show that Gd^{3+} and Ce^{3+} lie within the garnet phase. The ion radii of Gd^{3+} (0.94 Å) and Ce^{3+} (1.01 Å) are much larger than those of Al^{3+} (0.54 Å), so Gd^{3+} and Ce^{3+} are not incorporated in the Al_2O_3 structure.[33] The dodecahedron occupied by Lu^{3+} (0.86 Å) can accommodate ions with radii ranging from 0.830 to 1.290 Å.[34-35] Therefore, Gd^{3+} and Ce^{3+} ions enter in the LuAG crystal and eventually form the transparent Ce:LuGAG-Al_2O_3 biphasic nanoceramics.

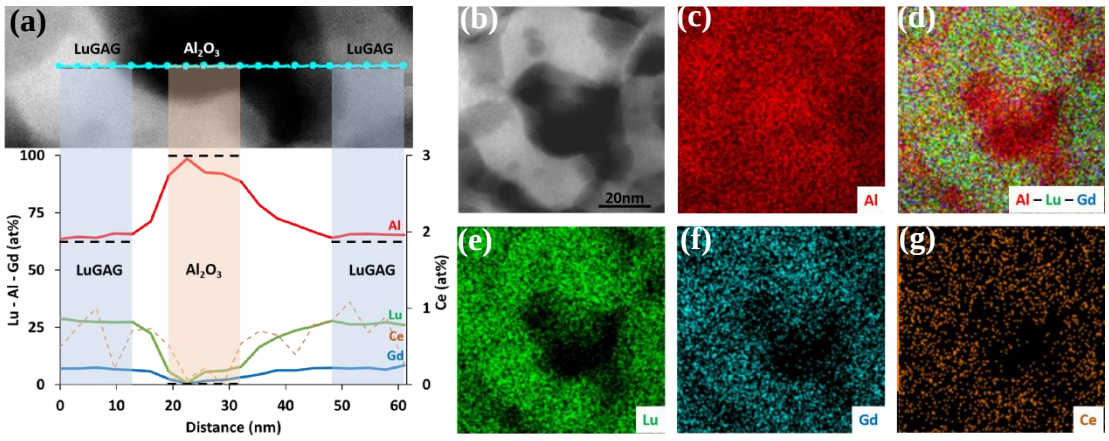

Figure 4. (a) STEM-HAADF micrograph and EDS line-scan results, (b-g) the corresponding STEM-HAADF image and EDS elemental maps of Al (red), Lu (green), Gd (blue), Ce (orange) and combined (Al-Lu-Gd) of transparent 0.3%Ce:LuGAG-Al_2O_3 nanoceramics (1100 ℃, 2 h).

Figure 5(a) presents the in-line transmittance of Ce dopped LuGAG-Al_2O_3 nanoceramics (Ce:LuGAG-Al_2O_3) with varied Ce^{3+} concentrations. It can be seen that the transmittance of transparent Ce:LuGAG-Al_2O_3 nanoceramics gradually decreases with the increase of Ce^{3+} doping concentration. As the Ce^{3+} doping concentration increases, the absorption intensity near 450 nm caused by the $4f \rightarrow 5d_1$ transition of Ce^{3+} gradually increases, thereby affecting the transmittance of the whole spectrum

range. When the Ce^{3+} doping content exceeds 0.3%, the transmittance 450 nm almost does not change any more, which indicates that the integrated absorption of Ce^{3+} has reached saturation. This is also confirmed by the absorption spectrum presented in **Figure S4**. The photoluminescence excitation (PLE) spectra and emission (PL) spectra of above Ce:LuGAG-Al_2O_3 transparent nanoceramics doped with different Ce^{3+} concentrations are shown in **Figure 5(b)**. The results show that all the transparent Ce:LuGAG-Al_2O_3 nanoceramics exhibit two typical broadband excitations, and the excitation peaks are located near 450 nm and 350 nm, corresponding to the $4f \rightarrow 5d_1$ and $4f \rightarrow 5d_2$ transitions of Ce^{3+}, respectively.[36-37] All the transparent Ce:LuGAG-Al_2O_3 nanoceramics exhibit a wide emission spectrum under the 450 nm excitation, and the emission peaks are located near 550 nm, corresponding to the $5d_1 \rightarrow 4f$ transition of Ce^{3+}, respectively.[38-39] Therefore, Ce:LuGAG-Al_2O_3 transparent nanoceramics can well absorb blue light with a wavelength of 450 nm, and emit green-yellow light when excited. With the increase of Ce^{3+} doping concentration, the emission peak has a significant red shift (546 nm→569 nm), which can be seen from the normalized PL spectra of Ce:LuGAG-Al_2O_3 nanoceramics in **Figure 5(c).** This is due to variable scattering effect, crystal field splitting and Stokes shift, which also exist in the transparent Ce:LuAG-Al_2O_3 nanoceramics. In addition, it can be seen from **Figure 5(d)** that the partial substitution of Gd^{3+} makes the emission spectrum of transparent Ce:LuAG-Al_2O_3 nanoceramics shift to red light (505 nm→545 nm), which is also found in Ce:YAG phosphor ceramics partially substituted by Gd^{3+}.[40] This is explained by the substitution of Lu^{3+} by Gd^{3+}, along which the coordination environment around Ce^{3+} evolves, which leads to the red shift of the emission wavelength of Ce^{3+}. Therefore, it appears that the Lu^{3+} for Gd^{3+} substitution coupled to tuning of the Ce^{3+} doping concentration leads to shift the emission peaks of transparent Ce:LuAG-Al_2O_3 nanoceramics from a green light region (λ_{em}=505 nm) to a orange-yellow light region (λ_{em}=570 nm). This is of great interest for further application of transparent Ce:LuGAG-Al_2O_3 nanoceramics for warm white lighting applications.

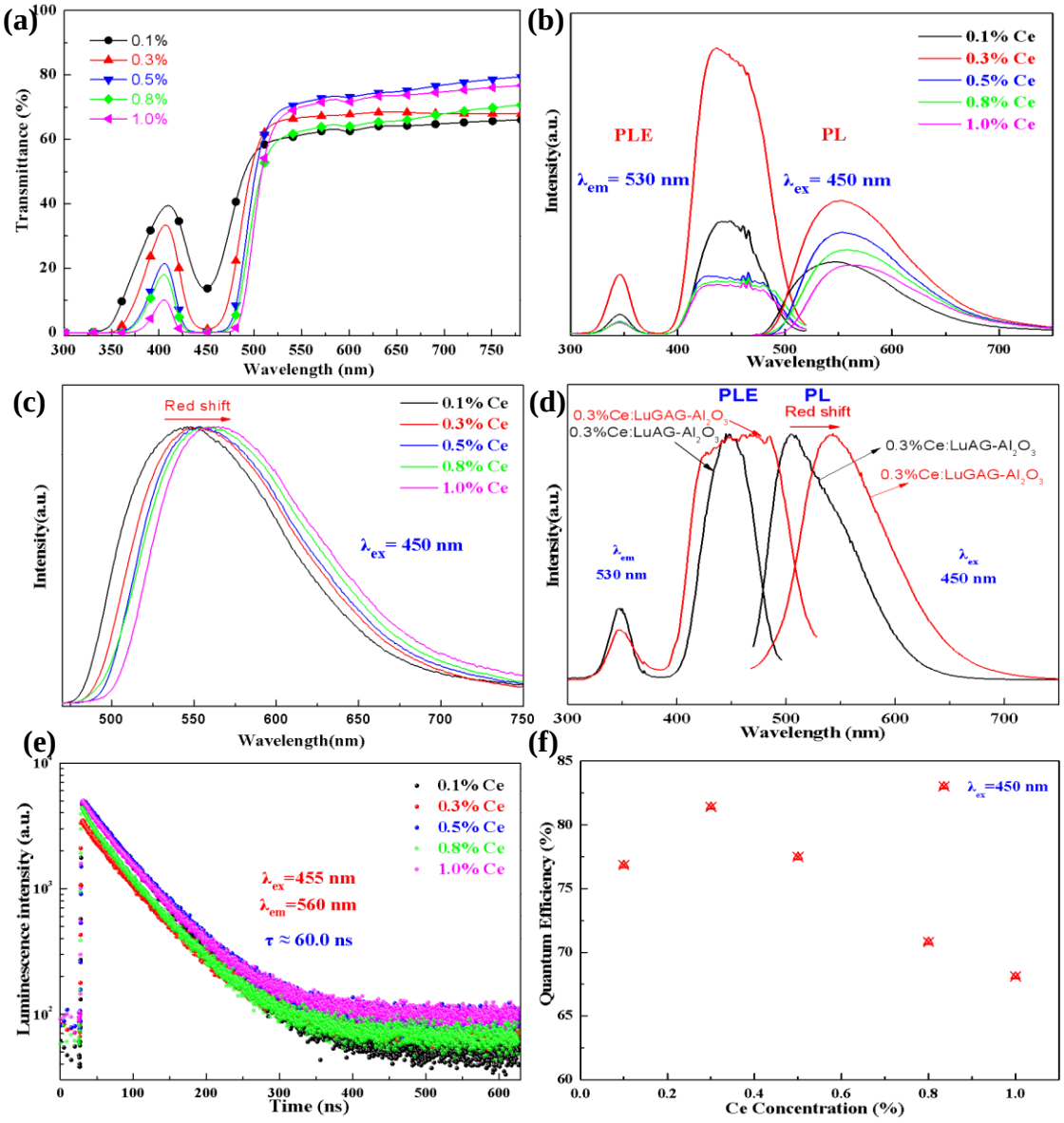

Figure 5. (a) In-line transmittance, (b) PLE spectra and PL spectra, and (c) normalized PL spectra of transparent Ce:LuGAG-Al_2O_3 nanoceramics, (d) normalized PLE spectra and PL spectra of 0.3%Ce:LuGAG-Al_2O_3 and 0.3%Ce:LuAG-Al_2O_3 transparent nanoceramics, (e) fluorescent decay curves for transparent Ce:LuGAG-Al_2O_3 nanoceramics, (f) quantum efficiency of transparent Ce:LuGAG-Al_2O_3 nanoceramics.

Figure 5(e) shows the fluorescent decay curves of transparent Ce:LuGAG-Al_2O_3 nanoceramics with different Ce^{3+} doping concentrations and from which the decay time can be obtained by single exponential fitting. The decay curves were recorded by monitoring the decay behavior of the Ce^{3+} emission peak at 560 nm under excitation at 455 nm wavelength. The results show that transparent Ce:LuGAG-Al_2O_3 nanoceramics exhibit a very short decay time (60 ns), which is close to transparent

Ce:LuAG-Al_2O_3 nanoceramics (55 ns), indicating that transparent Ce:LuGAG-Al_2O_3 nanoceramics can withstand the continuous excitation of blue light with high power density without light saturation. **Figure 5(f)** presents the quantum efficiency of transparent Ce:LuGAG-Al_2O_3 nanoceramics. When the doping concentration of Ce^{3+} is 0.3%, the quantum efficiency of transparent Ce:LuGAG-Al_2O_3 nanoceramic reaches its maximum, 81.4%. When the doping concentration of Ce^{3+} exceeds 0.3%, the quantum efficiency decreases gradually, indicating that concentration quenching occurs. The effect of temperature on the quantum efficiency of transparent 0.3% Ce:LuGAG-Al_2O_3 nanoceramics excited by 450 nm wavelength light has also been studied, as shown in **Figure S5**. The results show that the quantum efficiency of transparent 0.3%Ce:LuGAG-Al_2O_3 nanoceramics decreases with the increase of temperature, but when the temperature reaches 423 K, the quantum efficiency remains at 87.6% of room temperature, which is higher than that of commercial Ce:YAG phosphor (85.0%). These results demonstrate that transparent Ce: LuGAG-Al_2O_3 nanoceramics exhibit good thermal stability and can maintain good luminous efficiency at 243 K. Therefore the transparent Ce:LuGAG-Al_2O_3 nanoceramics meet the heat resistance required for high-power lighting applications.

3.3. Application for LED and LD lighting

In order to study the luminescence properties of transparent Ce:LuGAG-Al_2O_3 nanoceramics for LED lighting, ceramic sheets (Φ12 mm*1.0 mm) were combined with blue LED chip excitation (450 nm, 10 W) to build LED lighting devices. Electroluminescence (EL) spectrum and corresponding light color properties of transparent Ce:LuGAG-Al_2O_3 nanoceramics are shown in **Figure 6(a-e)**. The results show that the color rendering index fluctuates with the increase of Ce^{3+} doping concentration, due to the combined influence of transmittance and fluorescence efficiencies, showing a trend which first increases and then decreases. The highest color rendering index is 73.5 when the Ce^{3+} doping concentration is 0.8%. The color temperature of transparent Ce:LuGAG-Al_2O_3 nanoceramics gradually decreases from 5595 K to 4014 K with the increase of Ce^{3+} doping concentration from 0.1% to 1.0%.

However, the luminous intensity is consistent with the quantum efficiency: when the Ce^{3+} doping concentration is 0.3%, the luminous intensity of the transparent Ce:LuGAG-Al_2O_3 nanoceramics is the highest, and the luminous efficiency is 178.87 $lm \cdot W^{-1}$. **Figure 6(f)** shows the color coordinates of the above transparent Ce:LuGAG nanoceramics in the standard of CIE 1931. It can be seen that with the increase of Ce^{3+} doping concentration, the color coordinates gradually move from the green-yellow region to the orange-yellow region. The resulting point 3 (0.3628, 0.4253) and point 4 (0.3673, 0.406) are both in the warm white domain. The photographs of transparent Ce:LuGAG nanoceramics LED lighting devices are shown in **Figure 6(g)**, which clearly demonstrate the above color changes. The LuGAG-Al_2O_3 transparent nanoceramic doped with 0.8%Ce^{3+} demonstrate the best performance regarding warm white lighting with a high color rendering index of 73.5, a low color temperature of 4526 K and an excellent luminous efficiency of 143.98 $lm \cdot W^{-1}$.

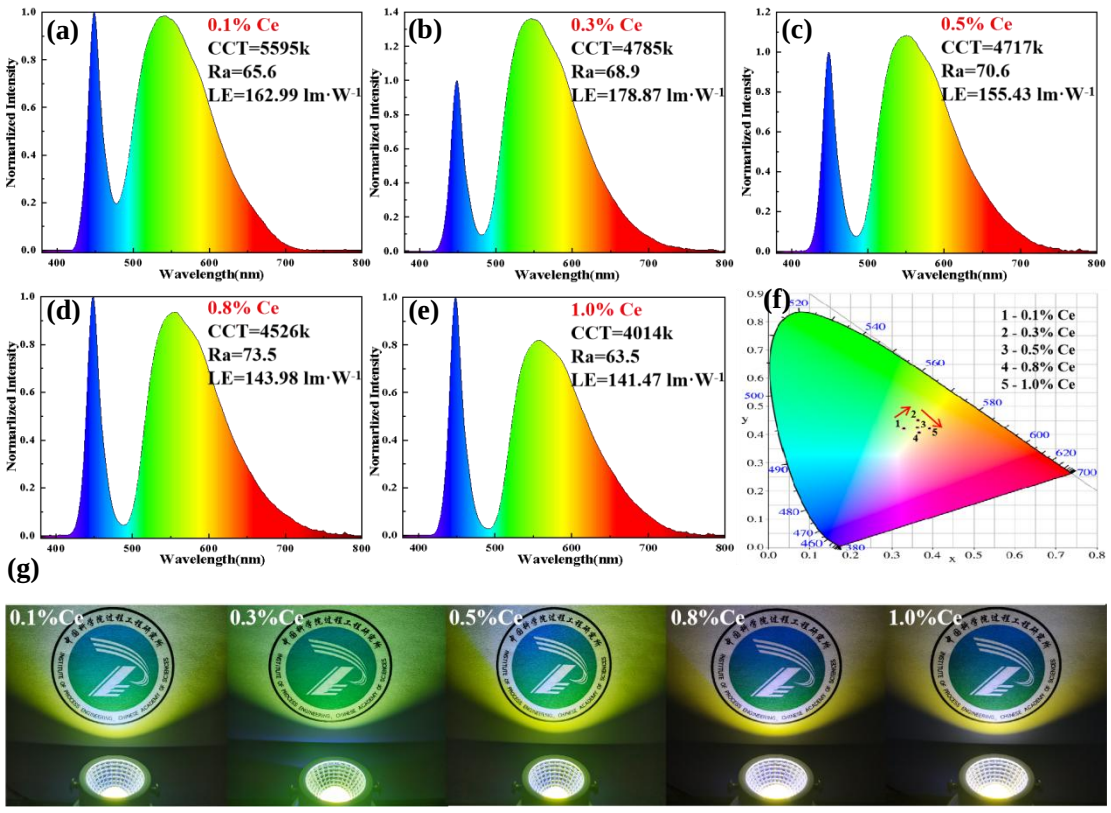

Figure 6. (a-e) EL spectra and corresponding light color properties, (f) CIE 1931 color coordinates and (g) photos of lighting of the LED devices fabricated by combining the blue-emitting InGaN chips and the Ce:LuGAG-Al_2O_3 transparent nanoceramics.

In order to further study the application of transparent Ce:LuGAG-Al_2O_3 nanoceramics in laser-diode-driven white lighting, the luminescence properties of nanoceramics under a blue laser excitation were measured in a reflective mode, and the incident power density was set as 5 W/mm^2. **Figure 7(a)** and **Figure 7(b)** show the EL spectrum and corresponding normalized EL spectrum of transparent Ce:LuGAG-Al_2O_3 nanoceramics under the excitation of blue laser at 450 nm wavelength. These spectra are consistent with the ones obtained from the LED devices illustrated in **Figure 6**. The maximum luminous intensity of Ce:LuGAG-Al_2O_3 nanoceramics under the excitation of blue laser is also observed for a 0.3% Ce^{3+} doping concentration. Moreover, with the increase of Ce^{3+} doping concentration, the EL spectrum shows obvious red shift, and the position of the emission peak shifts from 536 nm to 563 nm, which is due to the joint effect of Ce^{3+}-doped crystal field splitting intensification and 5d energy level centroid shift. **Figure 7(c)** presents the absorption (Abs.), internal efficiency (IE) and luminous efficiency (LE) of transparent Ce:LuGAG-Al_2O_3 nanoceramics. With the increase of Ce^{3+} doping concentration, the absorption gradually increases and reaches its maximum at 0.8% Ce^{3+}, which is 90.2%. When the Ce^{3+} doping concentration exceeds 0.8%, the Abs. begins to decrease, indicating that the absorption of blue light reaches the concentration threshold. The variation of IE and LE is consistent, and the maximum values, 63.7% and 240.04 $lm \cdot W^{-1}$ respectively, are obtained at 0.3% Ce^{3+}. As the concentration of Ce^{3+} increases to more than 0.3%, the IE and LE decrease, as a result of concentration quenching, which is due to the self-absorption between the luminescent centers caused by excessive doping. The color coordinates and the corresponding luminescent images are shown in **Figure 7(d).** With the increase of Ce^{3+} concentration, the color coordinate gradually moves from the green-yellow to the orange-yellow region, and finally to the blue-white region. When the Ce^{3+} doping concentration is 0.8%, the transparent Ce:LuGAG-Al_2O_3 nanoceramic emits warm

white light with coordinates of (0.3646,0.4096), the color temperature is 4611 K, the color rendering index is 65.4 and the LE is 161.29 $lm \cdot W^{-1}$. When the Ce^{3+} doping concentration exceeds 0.8%, the color coordinates of nanoceramics blue shift rapidly. This is due to the reduction of the fluorescence conversion efficiency of nanoceramics and the increase of the ratio of blue light with the excessive doping of Ce^{3+}.

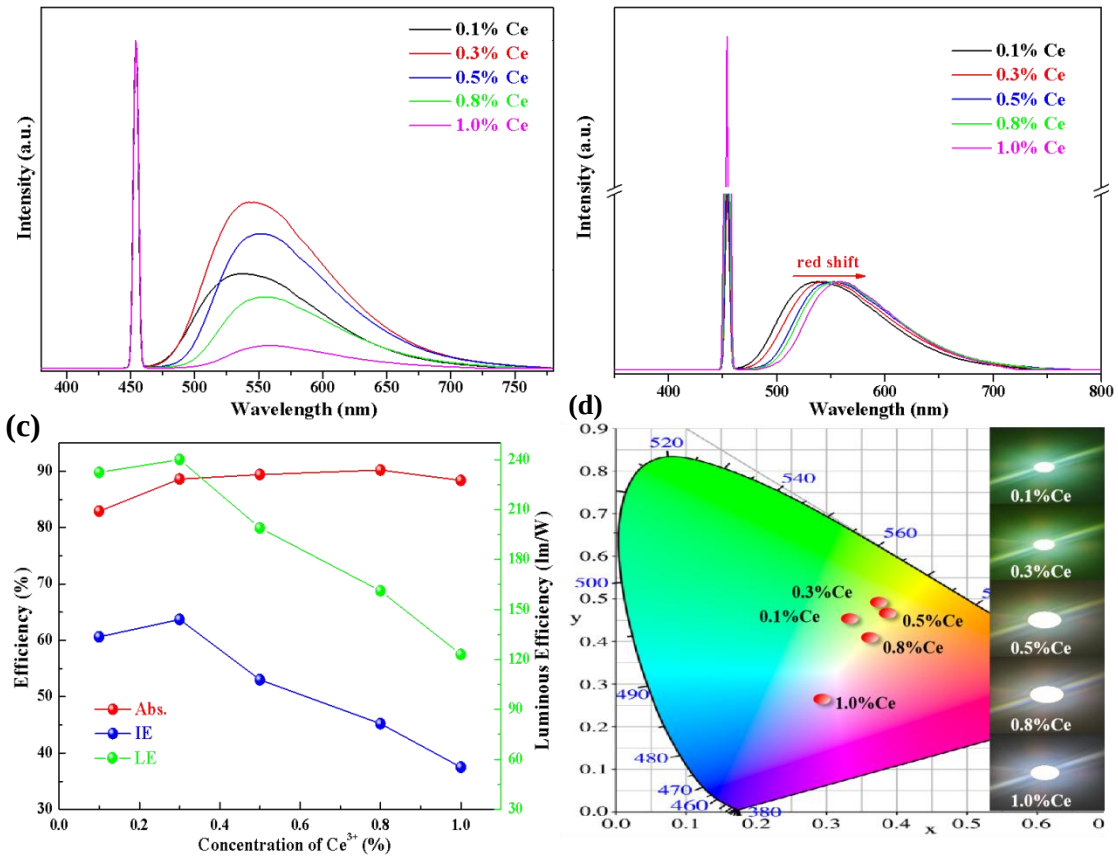

Figure 7. (a-b) EL spectra and corresponding normalized EL spectra, (c) absorption (Abs.), internal efficiency (IE) and luminous efficiency (LE), (d) CIE 1931 color coordinates of the Ce:LuGAG-Al_2O_3 transparent nanoceramics excited by blue laser. The corresponding luminescent images are indicated in the right inset.

At present, there are no reports on the preparation of Ce:LuGAG phosphor ceramics by replacing Lu^{3+} with Gd^{3+} for LED/LD lighting, although Gd^{3+} is often used to replace Y^{3+} to prepare Ce:GdYAG phosphor ceramics.[41-43] All the data presented above indicate that the transparent Ce:LuGAG-Al_2O_3 nanoceramics prepared in this work could solve the lack of red light component in the emission spectrum of transparent Ce:LuAG-Al_2O_3 nanoceramics. Moreover, the substitution of

Gd^{3+} and the doping of Ce^{3+} reduce the color temperature and enlarge the color rendering index of ceramics. Therefore, these transparent Ce:LuAG-Al_2O_3 nanoceramics are expected to be further used for high-power warm white LEDs/LDs.

4. Conclusion

Highly transparent LuGAG-Al_2O_3 nanoceramics with low cost were synthesized by full crystallization of A(Lu,Gd)28 bulk glasses at different temperatures, and the nanoceramics prepared at 1100 ^oC were mainly studied and analyzed. The density of the obtained transparent LuGAG-Al_2O_3 nanoceramics is 6.14±0.05 $g \cdot cm^{-3}$ and the grain size is 41±4 nm. The ceramic is formed of a dense biphasic three-dimensional network nanostructure. The dense LuGAG-Al_2O_3 nanoceramics present a perfect transparency from visible light to mid-infrared light, the transmittance especially reaches 82.3%@780 nm. Besides, the transparent LuGAG-Al_2O_3 nanoceramics show excellent mechanical properties, i.e., hardness and Young's modulus reach 23.4±0.5 GPa and 320.2±1.5 GPa respectively, which are about 10% higher than that of LuAG transparent ceramics obtained by vacuum sintering. Ce:LuGAG-Al_2O_3 transparent nanoceramics were synthesised and the maximum quantum efficiency of Ce:LuGAG-Al_2O_3 transparent nanoceramic reaches 81.4%. The good thermal stability (87.6%@423 K) indicates the potential of these materials for high power white lighting. Compared with transparent Ce:LuAG-Al_2O_3 nanoceramics, the emission spectrum shows an obvious red shift (505 nm→570 nm), which can supplement the red light component of transparent Ce:LuAG-Al_2O_3 nanoceramics. Combined with a blue-emitting InGaN chips (10 W), transparent 0.8%Ce:LuGAG-Al_2O_3 nanoceramics generate state of the art warm white light performance with a low color temperature of 4526 K, a high color rendering index of 73.5 and an excellent luminous efficiency of 143.98 $lm \cdot W^{-1}$. Under the excitation of blue laser-diode (5 W/mm^2), transparent 0.8%Ce:LuGAG-Al_2O_3 nanoceramic also reach the best warm white light performance, with a color rendering index of 65.4, a color temperature of 4611 K and a LE of 161.29 $lm \cdot W^{-1}$. Therefore, the transparent Ce:LuGAG-Al_2O_3 nanoceramics presented in this paper show great application prospects for high-power warm white LED/LD lighting.

Declaration of interests

The authors declare that they have no known competing financial interests or personal relationships that could have appeared to influence the work reported in this paper.

Author contributions

Jianqiang Li: Conceptualization, Methodology, Writing-review and editing, Supervision, Funding acquisition. **Mathieu Allix**: Conceptualization, Methodology, Writing-review and editing, Supervision. **Jie Fu**: Conceptualization, Methodology, Formal analysis and investigation, Writingoriginal draft preparation, Writing-review and editing, Supervision. **Ying Zhang**: Methodology, Resources, Writing-review and editing. **Shaowei Feng**: Methodology, Resources, Writing-review and editing. **Yongchang Guo**: Investigation, Resources. **Yafeng Yang**: Investigation, Resources. **Cécile Genevois**: TEM investigations, Resources. **Emmanuel Veron**: XRPD investigations, Resources. **Hui Wang**: Resources.

Acknowledgements

This work is financially supported by the National Natural Science Foundation of China (NSFC No. 51972304, No. 51971208), Beijing Municipal Science & Technology Commission, Administrative Commission of Zhongguancun Science Park (No. Z221100006722022), The Project of Scientific Experiment on Chinese Manned Space Station, and Chinese Academy of Sciences President's International Fellowship Initiative for 2021 (No. 2021VEA0012). The project benefitted from the microscopy facilities of the Platform MACLE-CVL which was co-funded by the European Union and Centre-Val de Loire Region (FEDER).

References

[1] E. F. Schubert, J. K. Kim. Solid-State Light Sources Getting Smart[J]. Science, 2005, 308(5726): 1274-1278.

[2] P. Pust, P. J. Schmidt, W. Schnick. A revolution in lighting [J]. Nature Materials, 2015, 14(5): 454-458.
[3] M. S. Shur, R. Zukauskas. "Solid-State Lighting: Toward superior illumination."[J]. Proceedings of the IEEE, 2005, 93(10): 1691-1703.
[4] J. M. Phillips, M. E. Coltrin, M. H. Crawford, et al. Research challenges to ultra-efficient inorganic solid-state lighting[J]. Laser & Photonics Reviews, 2007, 1(4): 307-333.
[5] M. H. Crawford. LEDs for solid-state lighting: performance challenges and recent advances[J]. IEEE Journal of Selected Topics in Quantum Electronics, 2009, 15(14): 1028-1040.
[6] Peng XL, Li SX, Liu ZH, et al. Phosphor Ceramics for High-power Solid-state Lighting[J]. Journal of Inorganic Materials, 2021, 36(8): 807-819.
[7] Li Jiang, Li Wanyuan, Liu Xin, et al. Research Progress on Phosphor Ceramics for Solid-state Lighting/Display[J]. Chinese Journal of Luminescence, 2021, 42(5): 580-604.
[8] G. L. Messing, A. J. Stevenson. Toward pore-free ceramics[J]. Science, 2008, 322 (17): 383-384.
[9] R. Won. Ceramic future[J]. Nature Photonics, 2008, 340(2): 1-2.
[10] H. Wang, Z. Huang, J. Qi, et al. A new methodology to obtain the fracture toughness of YAG transparent ceramics[J]. Journal of Advanced Ceramics, 2019, 8(3): 418-426.
[11] J. Ling, Y. Zhou, W. Xu, et al. Red-emitting YAG:Ce,Mn transparent ceramics for warm WLEDs application[J]. Journal of Advanced Ceramics, 2020, 9(1): 45-54.
[12] A. C. Berends, M. A. Haar, M. R. Krames. YAG:Ce^{3+} Phosphor: From Micron-Sized Workhorse for General Lighting to a Bright Future on the Nanoscale [J]. Chemical Reviews, 2020, 120(24): 13461-13479.
[13] Hu S, Qin X, Zhou G, et al. Luminescence characteristics of the Ce^{3+}-doped garnets: the case of Gd-admixed $Y_3Al_5O_{12}$ transparent ceramics[J]. Optical Materials Express, 2015, 5(12): 2902-2910.
[14] J. Xu, J. Wang, Y. Gong, et al. Investigation of an LuAG:Ce translucent ceramic synthesized via spark plasma sintering: Towards a facile synthetic route, robust thermal performance, and high-power solid state laser lighting[J]. Journal of the European Ceramic Society, 2018, 38(1): 343-347.
[15] K. Li, Y. Shi, F. Jia, et al. Low Etendue Yellow-Green Solid-State Light Generation by Laser-Pumped LuAG:Ce Ceramic[J]. IEEE Photonics Technology Letters, 2018, 30(10): 939-942.
[16] Ma C, Tang F, Chen J, et al. Spectral, energy resolution properties and green-yellow LEDs applications of transparent Ce^{3+}:$Lu_3Al_5O_{12}$ ceramics[J]. Journal of the European Ceramic Society, 2016, 36(16): 4205-4213.
[17] Xu J, Wang J, Gong Y, et al. Investigation of an LuAG:Ce translucent ceramic synthesized via spark plasma sintering: Towards a facile synthetic route, robust thermal performance, and high-power solid state laser lighting[J]. Journal of the European Ceramic Society, 2018, 38(1): 343-347.
[18] Y. L. Zhang, S. Hu, Z. J. Wang, et al. Pore-existing $Lu_3Al_5O_{12}$: Ce ceramic

phosphor:an efficient green color converter for laser light source[J]. Journal of Luminescence, 2018, 197(5): 331-334.
[19] Xinglu Qiana, Mingming Shia, Bobo Yang, et al. Thermostability and reliability properties studies of transparent Ce:GdYAG ceramic by Gd substitution for white LEDs[J]. Optical Materials, 2019, 94(5): 172-181.
[20] H. Shi, C. Zhu, J. Q. Huang, et al. Luminescence properties of YAG:Ce, Gd phosphors synthesized under vacuum condition and their white LED performances[J]. Optical Materials Express, 2014, 4(4): 649-655.
[21] S. Fujita, A. Sakamoto, S. Tanabe, Luminescence characteristics of YAG glass-ceramic phosphor for white LED[J]. IEEE Journal of Selected Topics in Quantum Electronics, 2008, 14(5): 1387-1391.
[22] Xiaobin Su, Kong Zhang, Qian Liu, et al. Combinatorial Optimization of $(Lu_{1-x}Gd_x)_3Al_5O_{12}:Ce^{3+}$ Yellow Phosphors as Precursors for Ceramic Scintillators[J]. ACS Combinatorial Science, 2011, 13(1): 79-83.
[23] S. H. Lee, E. R. Kupp, A. J. Stevenson, et al. Hot isostatic pressing of transparent Nd:YAG ceramics[J] Journal of the American Ceramic Society, 2009, 92(7): 1456-1463.
[24] I. Milisavljevic, M J Pitcher, J Q Li, et al. Crystallization of glass materials into transparent optical ceramics[J]. International Materials Reviews, 2023, 68(6): 648-676.
[25] A. Rosenflanz, M. Frey, B. Endres, et al. Bulk glasses and ultrahard nanoceramics based on alumina and rare-earth oxides[J]. Nature, 2004, 430(7001): 761-764.
[26] M. Allix, S. Alahraché, F. Fayon, et al. Highly transparent $BaAl_4O_7$ polycrystalline ceramic obtained by full crystallization from glass[J]. Advanced Materials, 2012, 24(41): 5570-5575.
[27] Alahraché S, Al Saghir K, Chenu S, et al. Perfectly transparent $Sr_3Al_2O_6$ polycrystalline ceramic elaborated from glass crystallization[J]. Chemistry of Materials, 2013, 25(20): 4017-4024.
[28] K. Al Saghir, S. Chenu, M. Allix, et al. Transparency through structural disorder a new concept for innovative transparent ceramics[J]. Chemistry of Materials, 2015, 27(2): 508-514,
[29] Ma XG, Li XY, Li JQ, et al. Pressureless glass crystallization of transparent yttrium aluminum garnet-based nanoceramics[J]. Nature Communications, 2018, 9(1): 1175.
[30] Jie FU, Shaowei FENG, Ying ZHANG, et al. $Ce^{3+}:Lu_3Al_5O_{12}$-Al_2O_3 optical nanoceramic scintillators elaborated via a low-temperature glass crystallization route[J]. Journal of Advanced Ceramics, 2023, 10(5): 55-67.
[31] Deubener J, Allix M, Davis M J, et al. Updated definition of glass-ceramics[J]. Journal of Non-Crystalline Solids, 2018, 501(23): 3-10.
[32] Rüssel, C. Nanocrystallization of CaF_2 from $Na_2O/K_2O/CaO/CaF_2/Al_2O_3/SiO_2$ glasses[J]. Chemistry of Materials, 2005, 17(23): 5843-5847.
[33] George N C, Denault K A, Seshadri R. Phosphors for solid-state white lighting[J]. Annual Review of Materials Research, 2013, 43(1): 481-501.
[34] Song Z, Zhou D, Liu Q. Tolerance factor and phase stability of the garnet

structure[J]. Acta Crystallographica Section C-Structural Chemistry, 2019, 75(10): 1353-1358.
[35] Song Z, Xia Z, Liu Q. Insight into the relationship between crystal structure and crystal-field splitting of Ce^{3+} doped garnet compounds[J]. The Journal of Physical Chemistry C, 2018, 122(6): 3567-3574.
[36] Guo D D, Ma B J, Liu H. Bright YAG:Ce Nanorod Phosphors Prepared via a Partial Wet Chemical Route and Biolabeling Applications[J]. Acs Applied Materials & Interfaces, 2016, 8(19): 11990-11997.
[37] Na Zhang, Dajian Wang, Lan Li, et al. YAG:Ce Phosphors for WLED via Nano-Pesudoboehmite Sol-Gel Route[J]. Journal of Rare Earths, 2006, 24(3): 294-297.
[38] Haranath D, Chander H, Sharma P, et al. Enhanced luminescence of $Y_3Al_5O_{12}:Ce^{3+}$ nanophosphor for white light-emitting diodes[J]. Applied Physics Letters, 2006, 89(17): 173118.
[39] Young Hyun Song, Eun Kyung Ji, Byung Woo Jeong, et al. Design of laser-driven high-efficiency Al_2O_3/YAG:Ce^{3+} ceramic converter for automotive lighting: Fabrication, luminous emittance, and tunable color space[J]. Dyes and Pigments, 2017, 139(5): 688-692.
[40] Hu C, Shi Y, Feng X, et al. YAG:Ce/(Gd,Y)AG:Ce dual-layered composite structure ceramic phosphors designed for bright white light-emitting diodes with various CCT[J]. Optics Express, 2015, 23(14): 18243-18255.
[41] Liu X, Zhou H, Hu Z, et al. Transparent Ce:GdYAG ceramic color converters for high-brightness white LEDs and LDs[J]. Optical Materials, 2019, 88: 97-102.
[42] Wen B, Zhang D F, Jiang B, et al. Thermal conductivity of Ce^{3+} doped $(Y,Gd)_3Al_5O_{12}$ ceramic phosphor[J]. Journal of Luminescence, 2020, 221: 116886.
[43] Qian X, Li Y, Shi M, et al. Color converter based on transparent Ce:YAG ceramic by different package structure for high-power white LED[J]. Ceramics International, 2019, 45(17): 21520-21527.

Supporting Information

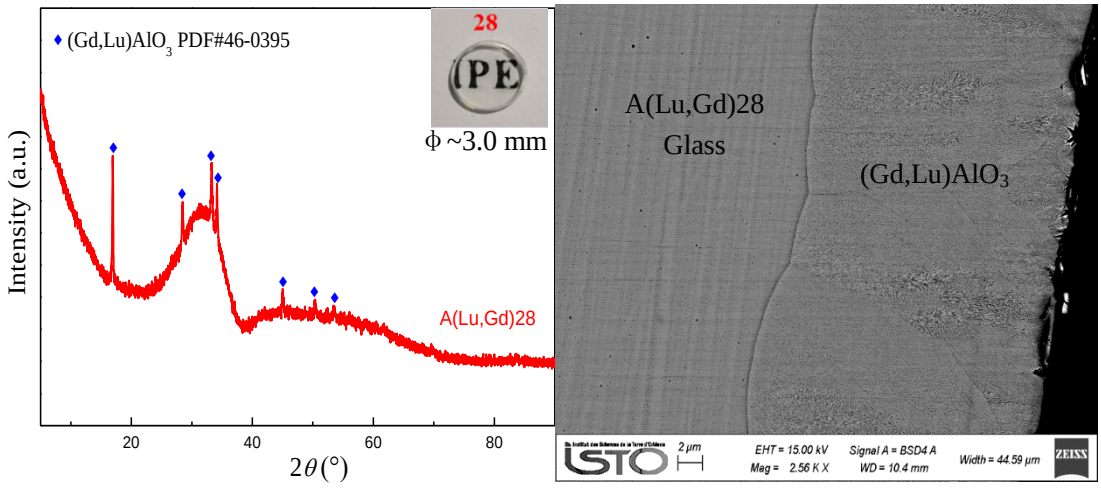

Figure. S1 XRPD pattern and SEM of the A(Lu,Gd)28 glass synthesized through containerless solidification process (the thickness of $(Gd,Lu)AlO_3$ is ~10 μm).

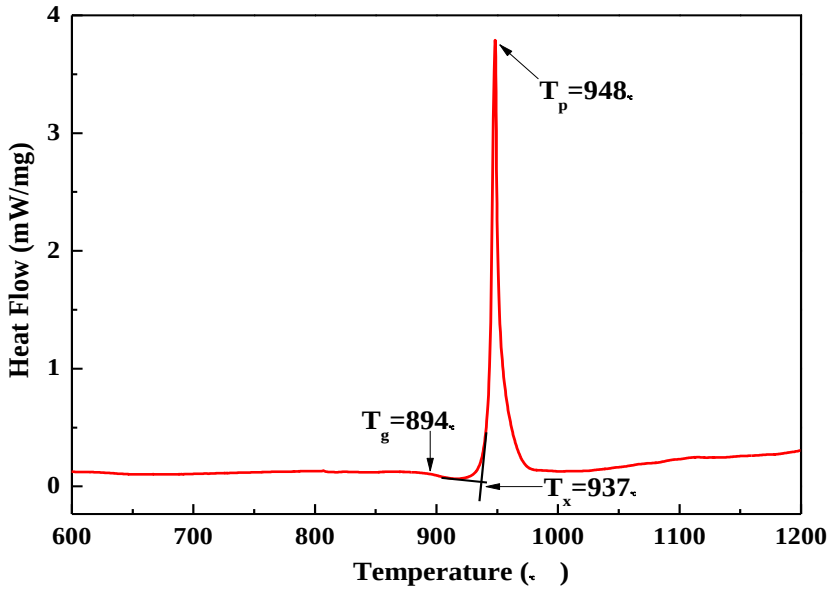

Figure. S2 DSC curve of the A(Lu,Gd)28 glasses (glass beads) synthesized through containerless solidification process.

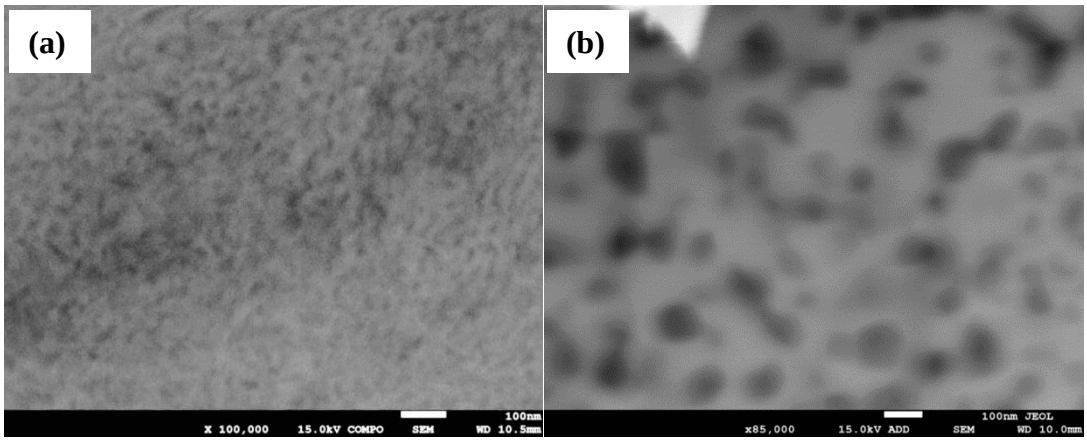

Figure. S3 SEM backscattering images of transparent ceramics crystallized from A(Lu,Gd)28 bulk glasses at (a) 1100 °C and (b) 1300 °C.

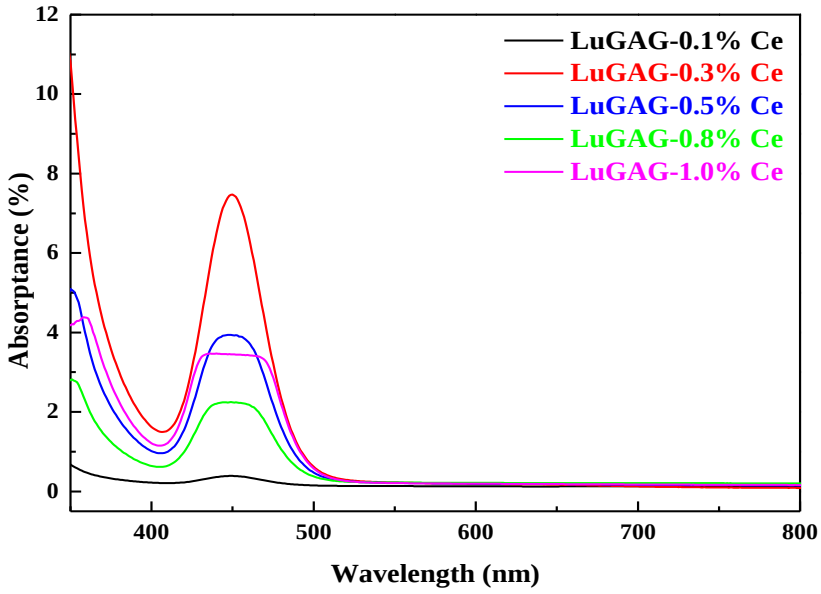

Figure. S4 Absorption spectrum of Ce:LuGAG-Al_2O_3 transparent nanoceramics with different Ce^{3+} contents.

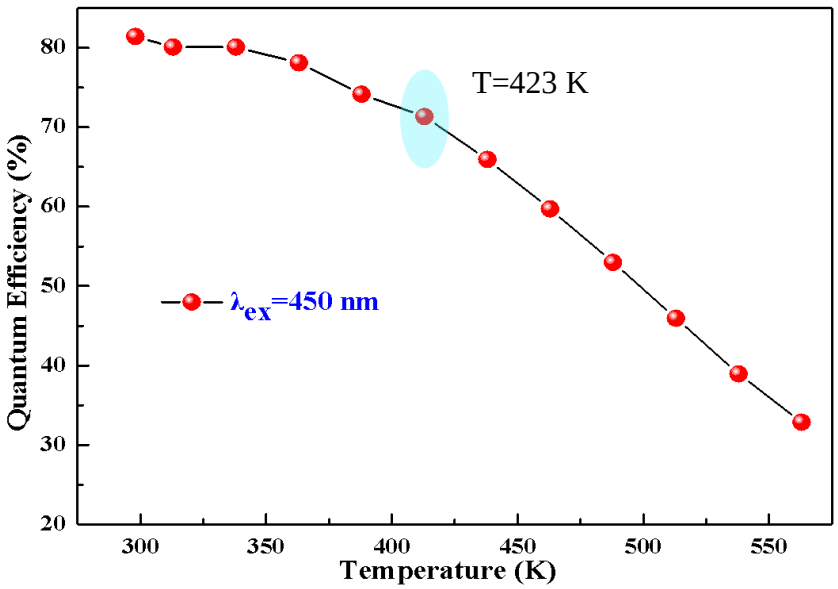

Figure. S5 Variable temperature quantum efficiency of 0.3%Ce:LuGAG-Al_2O_3 transparent nanoceramics.